SUB-BAND ANALYSIS IN UWB RADIO CHANNEL MODELING

Lassi Hentilä
Centre for Wireless Communications
P.O. Box 4500
90014 University of Oulu
Finland

Veikko Hovinen
Telecommunication Laboratory
P.O. Box 4500
90014 University of Oulu
Finland

Matti Hämäläinen
Centre for Wireless Communications
P.O. Box 4500
90014 University of Oulu
Finland

ABSTRACT

The paper presents ultra wideband (UWB) channel measurements from 3.1 to 8.0 GHz in office and lecture hall environments carried out at the premises of University of Oulu. Both line-of-sight (LOS) and non-LOS (NLOS) channels were measured having transmitter-receiver separation from 4 to 10 m. Channel parameters that are corresponding to the modified IEEE 802.15.3a model are extracted from the measurement data. In addition, delay spread and path loss are studied. In the study, the measured frequency band is divided into sub-bands and analysed separately. The effect of frequency over the UWB band on the channel statistics is pointed out.

I. INTRODUCTION

The performance prediction and simulation of new communication systems based on the UWB technology require a deep knowledge of a physical channel. The recent measurements carried out to characterise the UWB channel on the campus area of the University of Oulu are based on the frequency domain approach, whereas the modelling has been done in the time domain. In the previous UWB channel models the statistical properties of the channel have been studied using the full measured frequency band. This approach assumes that the frequency does not affect to the channel statistics. In this paper, the analysis is based on selection of three 100 MHz sub-bands, one in the centre of the original UWB frequency band and the two others at the low and high ends of the band. The channel parameters are extracted separately for the sub-bands and for the full band.

II. MEASUREMENT SETUP

The channel measurement system used in this work is presented in detail in [1]. The sounder consists of a vector network analyser (VNA), a wideband amplifier, a wideband conical monopole antenna pair, coaxial cables and a control computer as illustrated in Fig. 1. In addition, a stepped track was used at the receiver end to enable antenna movement. Table 1 lists the main parameters of the measurements.

The selected 4.9 GHz frequency band from 3.1 GHz to 8.0 GHz falls within the FCC spectrum mask from 3.1 GHz to 10.6 GHz for UWB transmission. The number of frequency points per sweep is 1601.

In order to enhance the antenna positioning accuracy, a stepped track (antenna carriage) was used at the RX end. During the measurements, the control PC instructs the RX antenna carriage to move along the rail in 1.0 cm steps. The length of the track is 2.35 m, giving 235 different antenna positions. The TX antenna was in a fixed position during the measurement campaign. The antenna heights at both ends were 1.34 m, measured from the radiation centres of the antennas.

The stepped track at the RX end also made it possible to consider the measurement data as if there had been a single input, multiple output (SIMO) channel.

Table 1. Measurement setup parameters

Parameter	**Value**
Frequency band	3.1 to 8.0 GHz
Bandwidth	4.9 GHz
IF bandwidth of the VNA	3.0 kHz
Number of points over the band	1601
Sweep time	800 ms
Dynamic range	90 dB
Average noise floor	-120 dBm
Transmit power	+5 dBm
Amplifier gain (min/max)	25 / 36 dB
Amplifier delay	0.60 ns
Antenna gain (typical)	0 dBi
TX cable loss (min/max)	3.5 / 8.0 dB
RX cable loss (min/max)	0.6 / 1.0 dB
EIRP (max)	26.2 dBm

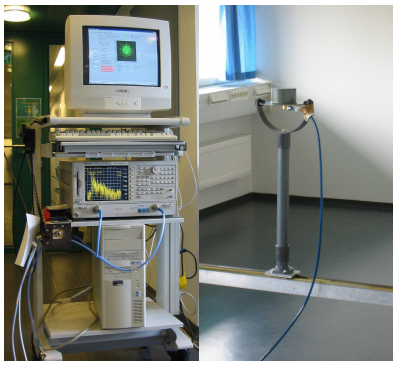

Figure 1. The measurement setup: the trolley and the antenna on the carriage.

III. MEASUREMENT ENVIRONMENTS

The measurements were carried out at spatially distributed locations, mainly in the Tietotalo building at the University of Oulu. In addition, some measurement data was collected from lecture halls on the main university campus. In the Tietotalo building the transmitting antenna was placed in room TS440. The track of the receiving antenna was located in two rooms adjacent to TS440, which were TS441 and TS472. A 1.5 m wide corridor borders all three rooms, so all of the measured direct links included two walls. The wall material of rooms TS440 and TS441 is

plasterboard and of room TS472, iron-strengthened concrete.

This construction contains different measurement distances from 4 m to 10 m and two kinds of environments for analysis: $NLOS_1$ and $NLOS_2$. $NLOS_1$ contains non-line-of-sight with two plasterboard walls between the antennas. $NLOS_2$ contains plasterboard and concrete walls.

Three track positions in TS441 and two in TS472 give five positions. Given that each track position has 235 antenna positions, the total number of measurement positions is 705 in the $NLOS_1$ case and 470 in the $NLOS_2$ case. Fig. 2 illustrates the measurement environment in the Tietotalo building.

The LOS and part of the $NLOS_1$ measurements were performed in the university lecture halls SÄ118, L5 and L6. The TX antenna was located in a fixed position 2 to 4 metres from the wall. The RX end was moved along a straight line about 1 m from the wall both inside and outside the room. The wall between the TX and RX was a single layer brick wall in the case of SÄ118 and L5 and a solid double brick wall in the L6 case.

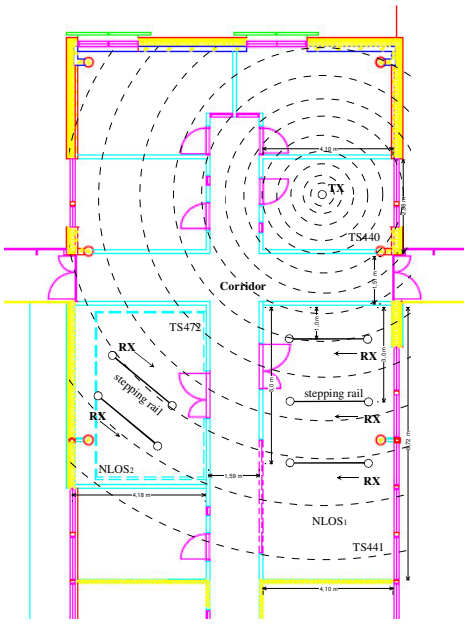

Figure 2. Floor plan of the office building (Tietotalo), where the channel measurements were carried out.

IV. Data Post-Processing

Before the channel model was extracted from the raw measurement data, various data processing and signal analysis stages were performed. Power delay profiles (PDP) were constructed using all signal data collected in different rooms and positions during the measurement campaign. The effects of small-scale and large-scale statistics were analysed separately. Small-scale statistics were extracted from one track position containing 235 antenna positions. Large-scale statistics were achieved by merging all the track positions into the same pool and averaging the PDPs spatially.

An IFFT was used to transform the measured frequency domain data to the time domain. The IFFT is usually taken directly from the measure raw data vector (typical method). There are two common techniques for converting the signal to the time domain, which both lead to approximately same results. The first approach [2] is based on Hermitean signal processing, which gives a better pulse shape. The second approach (conjugate approach) has been found to be an easier and more efficient way to obtain the same pulse shape accuracy. The conjugate approach, which is illustrated in Fig. 3, involves taking the conjugate reflection of the passband signal without zero padding. Using only the left side of the spectrum, the signal is converted using an IFFT with the same window size as in the Hermitean approach. The result is practically the same as that stated in the Hermitean case, as can be seen in Fig. 4. The conjugate method is more efficient in data processing, since the desired number of zeros is added automatically by the IFFT function. In this method, 3 dB of power needs to add in order to maintain the channel energy, since the spectrum is one-sided.

Windowing was used to obtain the arrival time of the first path in the PDP, but the channel model parameters were extracted without windowing. Windowing sharpens the edge of the PDP, making positioning of the arrival time easier. In addition, windowing distorts the frequency spectrum and underestimates the delay spread.

For all impulse responses $h(t)$, normalisation is performed by setting the channel energy at each position to unity. The normalised impulse response IR_n is obtained by

$$IR_n = \frac{h(t)}{\sqrt{\sum_{k=1}^{L} |h(t_k)|^2}}. \quad (1)$$

The PDP is then a squared value of the IR_n. The normalisation makes it possible to compare the statistics of the PDPs that have been measured at different positions.

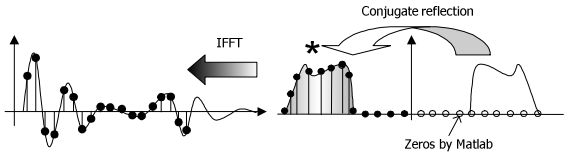

Figure 3. Idea of the conjugate approach.

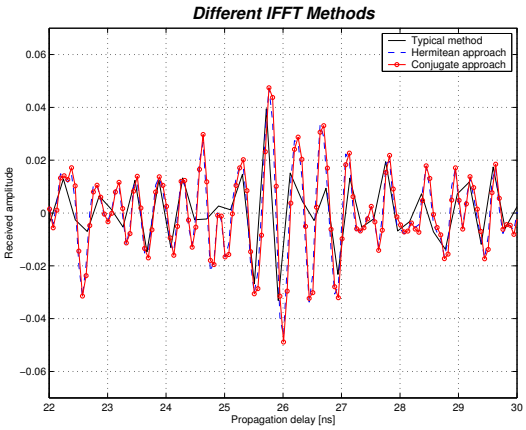

Figure 4. Impulse responses of the channel using different IFFT methods.

V. CHANNEL MODELLING

A. *Multipath Amplitude Fading*

Amplitude fading in a multipath radio channel may follow different distributions depending on the measurement environment. Rayleigh and lognormal distributions are the best candidates in a NLOS channel and Rice in a LOS channel [3]. The analysis here was divided into a small-scale and a large-scale statistics. The small-scale area was chosen to be 43 wavelengths, calculated according to the 5.5 GHz centre frequency. That contains 235 positions on the track and 1880 sweeps altogether. Amplitude fading distributions were calculated to show the variability of the amplitude through the small-scale PDPs. A comparison was done by fitting the measured amplitudes to lognormal, Rayleigh and Rice distributions. Kolmogorov-Smirnov test [4] is used to show the reliability of the fit. For the measured data, a significance of 1 % is used to evaluate the reliability of the fit. Traditionally, 1 % and 5 % are the most commonly used values. Tables below show, how different CDFs fit to the data. Table 2 depicts all of the measurement environments from LOS to $NLOS_2$ (c.f. Fig. 2) using the full measured band. Table 3 compares the fit in the case of LOS with different sub-bands.

Table 2. Comparison of pass rates of multipath fading distributions using full band

FULL BAND	Pass rate of lognormal (%)	Pass rate of Rayleigh (%)	Pass rate of Rice (%)
LOS (lecture hall)*	99.5	52.4	45.6
$NLOS_1$ (office)**	83.3	13.6	0.8
$NLOS_2$ (office)**	78.1	7.6	1.3

* Large-scale

** Small-scale

Table 3. Comparison of pass rates of multipath fading distributions in SÄ118

Large-scale SÄ118 – LOS	Pass rate of lognormal (%)	Pass rate of Rayleigh (%)	Pass rate of Rice (%)
Lower sub-band	96.8	71.0	41.9
Median sub-band	96.8	58.1	64.5
Upper sub-band	96.8	67.7	32.3
Full band	99.5	52.4	45.6

It is evident from the tables that the lognormal distribution fits best to the data in all the cases. The same result was obtained in some previous UWB measurement campaigns, such as [2] and [5]. When observing the large-scale sub-band approaches, it can be seen from Table 3 that the Rayleigh distribution improves the percentage value in the LOS case in both sub-bands. This results from the fact that when the bandwidth is decreased, more signal components merge into one path in the PDP and thus the statistical process of the given path amplitudes becomes more and more Rayleigh-like. Proof of the Rayleigh nature is also provided in various previous wideband radio channel measurements, which are discussed in detail in [3]. Fig. 5. show the change in the delay resolution in the PDP when the bandwidth is decreased.

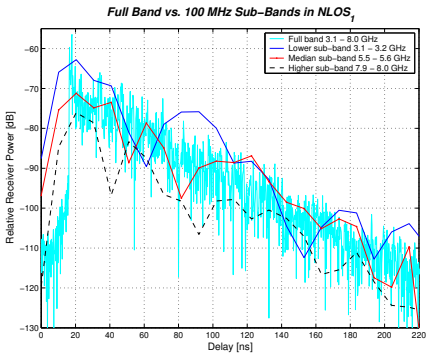

Figure 5. PDP of different sub-bands in $NLOS_1$.

B. *Path Loss*

In this work, path loss was studied in all of the measured environments. The path losses were calculated by averaging the transfer functions over the frequency band as a function of distance according to [6]

$$PL(d) = -10\log_{10}\left(\frac{1}{1601}\sum_{i=1}^{1601}\left|H(d,f_i)\right|^2\right), \qquad (2)$$

where $H(f_i)$ is channel transfer function.

Averaging over frequencies can be explained by the fact that the path loss is relatively insensitive to frequency. Path loss exponent in indoor UWB LOS radio channel can be below that of a free space loss. This can be explained by the fact that UWB indoor radio channel is very rich with reflected signals from the walls. Fig. 6. show the excess path loss of the different sub-bands in NLOS case. It evidently proves, as expected, smaller path loss for the lower sub-band and vice versa.

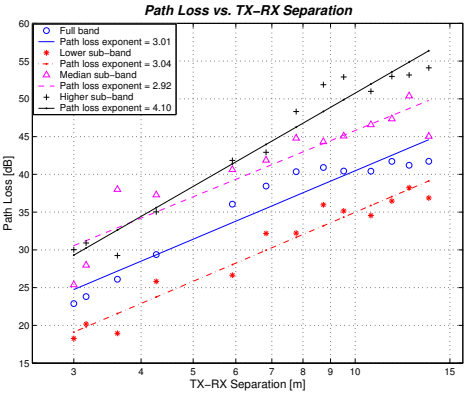

Figure 6. Excess path loss of the different sub-bands in the case of NLOS.

C. *Multipath model*

The multipath model was obtained by investigating the multipath propagated signals in the PDP. When considering the basic tapped-delay-line model, which gives relative power values to the taps with a given delay, the number of taps is directly proportional to the complexity of the model. The UWB signal results in a PDP with very high accuracy, and therefore the number of paths in the model should be a large value. This is one reason why the

tapped-delay-line model was not generated in this work. Another and more reasonable motive is that the measured PDPs have distinct clusters. The proposed model for the channel having the cluster phenomenon is an IEEE 802.15.3a model defined in [7]. The model presented in [8] is modified in order to fit the measured UWB channel data to the model. As presented in Tables 2 and 3, the amplitude seems to be lognormally distributed rather than Rayleigh distributed. In addition, each cluster and the rays inside the cluster are assumed to have independent fading. Fig. 7. shows the idea of the IEEE 802.15.3a channel model. The figure is a compound from [7] and [8].

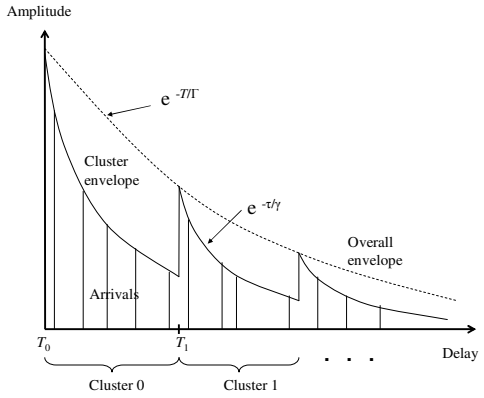

Figure 7. Illustration of the IEEE 802.15.3a channel model.

A couple of key parameters, including the cluster and ray arrival rates (Λ and λ), the cluster and ray decay factors (Γ and γ) and the standard deviations of the fading and shadowing terms (σ_1, σ_2 and σ_x) define the model. The model parameters shown in Table 4 were found by searching reasonable values for them that fit to our measured data. Using the parameters from the table one hundred channel realisations were constructed, as shown in Fig. 8.

Table 4. Modified IEEE 802.15.3a model parameters and characteristics

Model Parameters	**LOS**	**NLOS$_1$**	**NLOS$_2$**
Λ [1/ns]	0.05	0.1	0.05
λ [1/ns]	16	6	9
Γ [ns]	16	19	24
γ_r [ns]	1.03	2	5
σ_1, σ_2 [dB]	3.4	3.4	3.4
σ_x [dB]	2	2	2
Model Characteristics			
τ_m [ns]	8.8	15.0	18.9
τ_{RMS} [ns]	14	18	21
$NP_{10\,dB}$	9	16	27
$NP_{85\,\%}$	15	39	65
Channel energy mean [dB]	-0.6	-0.5	0.1
Channel energy std [dB]	2.1	2.3	2.4

D. RMS Delay Spread and Mean Excess Delay

RMS delay spread is a time domain parameter typically used to give an idea of the channel characteristics. All time domain parameters were obtained from the PDPs by taking into account the thresholds presented in Fig. 9. The initial delay was estimated first. The most accurate way to estimate the initial delay is to compare the exact distance measured with a laser meter and the position of the corresponding path from the measured data. The average noise level was typically around –60 dB above the maximum multipath component in the normalised PDP, but we estimated it separately for all of the cases by averaging the evident noise level before the first multipath component arrives [5]. RMS delay spread and mean excess delay were then calculated from the data, which is 15 dB above the noise level. A dynamic range of approximately 45 dB was then obtained for the final channel modelling.

RMS delay seems to be typically between 14 ns and 21 ns in indoor environments. A LOS channel provides 14 ns as an average, NLOS$_1$ provides 18 ns and NLOS$_2$, which can be referred to as an extreme NLOS, provides 21 ns as an average value. The values for indoors, as presented in the model in [7], are 5.28 ns, 14.28 ns and 25 ns for the same type of channels, respectively. The values in [7] are proposed for the same distances that were measured in this work, but their environmental parameters differ.

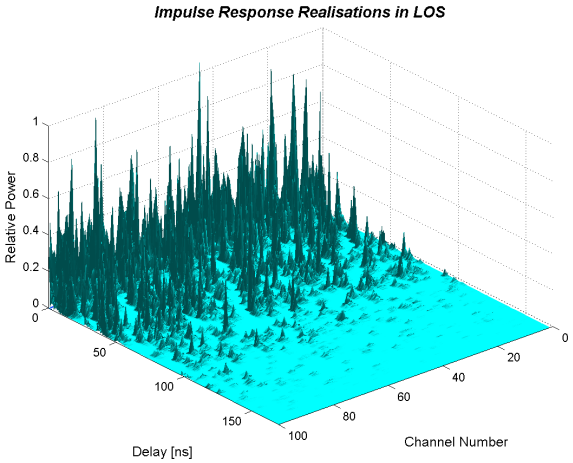

Figure 8. One hundred LOS impulse response realisations generated with the parameters shown in Table 4.

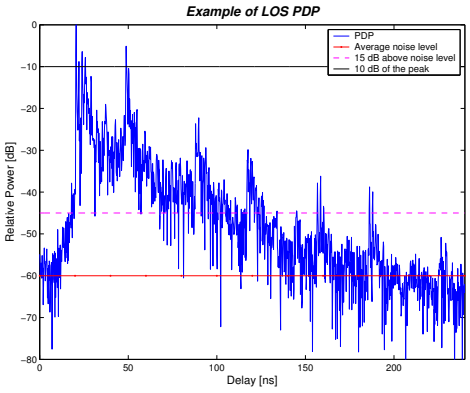

Figure 9. Typical power delay profile in an indoor LOS channel (from the measurements).

The mean excess delay is 8.8 ns for LOS, 15 ns for NLOS$_1$ and 18.9 ns for NLOS$_2$. The values in the model in [7] are 5.0 ns, 14.18 ns and undefined, respectively. Pre-

vious measurements provide in the order of 30 ns for the extreme NLOS case [7]. One reason for the difference between the measured value and the value in the model in [7] might be the way of positioning the time of arrival of the first path in the PDP. If the positioning is based only on the choice of the first path after the noise level is cut, the mean excess delay increases. The real position of the arrival time of the first path in the PDP is later than the noise-cut position.

The delay spread parameters of the separate sub-bands are presented in Table 5, where the difference from the full band is evident. The values in Table 5 can also be compared to the results of the previous wideband measurement campaigns. For example, in [9] with a 100 MHz bandwidth, the RMS delay spread is 33 ns and 48 ns for 90 and 60 MHz centre frequencies, respectively. With the lower centre frequency, signal attenuation is reduced, which makes the RMS delay spread larger. However, this is not the case with the UWB measurements and its sub-band observations, as depicted in Table 5.

Table 5. Comparison of delay spread values for separate sub-bands

LOS, L5 / L6	τ_m [ns]	τ_{RMS} [ns]
Lower sub-band (100 MHz)	10.9	13
Median sub-band (100 MHz)	9.9	15
Upper sub-band (100 MHz)	15.5	16
Full band (4.9 GHz)	8.4	14
$NLOS_1$, TS 441		
Lower sub-band (100 MHz)	12.4	18
Median sub-band (100 MHz)	13.3	17
Upper sub-band (100 MHz)	9.4	16
Full band (4.9 GHz)	10.0	16
$NLOS_2$, TS 472		
Lower sub-band (100 MHz)	29.8	21
Median sub-band (100 MHz)	26.7	26
Upper sub-band (100 MHz)	29.6	43
Full band (4.9 GHz)	15.3	22

E. Number of Paths

The number of paths within 10 dB of the peak counted in the PDP is a significant parameter when discussing the channel models. It has a direct relationship to the complexity of the channel simulator and the whole communication system planning. If the number of paths is high, system simulations take longer time. In addition, the receiver structure becomes more complicated to be able to pick up all of the desired multipath arrivals.

The number of paths within 10 dB of the maximum multipath component in the measured data is about 10 to 30 in the cases from LOS to $NLOS_2$. The number of paths containing 85 % of the energy is from 15 to 65, including the environments from LOS to $NLOS_2$, respectively. Both parameters were listed in Table 4.

CONCLUSIONS

When analysing the three 100 MHz sub-bands of the measured UWB channel, some interesting findings were attained. The amplitude fading distributions seem to vary in the different sub-bands, which can be seen in the pass rates of the Kolmogorov-Smirnov test. In the hypothesis tests, Rayleigh, Rice and lognormal distributions were considered. The best fitting distribution for the UWB was the lognormal, also for the 100 MHz sub-bands, even though the Rayleigh and Rice distributions increased the percentage value in these cases.

The free space loss model seems to be a rather good outline of the path loss in the LOS indoor UWB channels. The path loss exponent increases slightly above two when the LOS changes into a typical NLOS. The most distinct difference compared to free space loss is the excess attenuation caused by the furniture, walls and other obstacles.

The multipath channel model was obtained from the data by investigating the average PDPs of different environments. A modified IEEE 802.15.3a channel model based on the Saleh-Valenzuela channel model was constructed. The signal components in the PDPs arrive in distinct clusters, making the IEEE 802.15.3a model a good candidate.

VI. ACKNOWLEDGEMENTS

This research is funded by the National Technology Agency of Finland (Tekes), Elektrobit Ltd. and the Finnish Defence Forces. Authors would like to thank the sponsors for their support. Many thanks go also to the people who have contributed the work, especially Professors Seppo Karhu and Jari Iinatti and M.Sc. Niina Laine.

REFERENCES

[1] M. Hämäläinen, T. Pätsi and V. Hovinen "Ultra Wideband Indoor Radio Channel Measurements," *in Proceedings of the 2nd Finnish Wireless Communications Workshop*, 2001, 5 p.

[2] J. Keignart and N. Daniele "Channel Sounding and Modelling for Indoor UWB communications," *in Proceedings of the First International Workshop on Ultra Wide-band Systems*, 2003, 5 p.

[3] H. Hashemi "The Indoor Radio Propagation Channel," *Proceedings of the IEEE 81*, 1993, pp. 943–968.

[4] R. Vaughan and J. B. Andersen "Channels, Propagation and Antennas for Mobile Communications," *The IEE Electromagnetic Waves Series 50*, London, 2003, 753 p.

[5] D. Cassioli, M.Z. Win and A.F. Molisch "The Ultra-Wide Bandwidth Indoor Channel: From Statistical Model to Simulations," *IEEE Journal on Selected Areas in Communications*, 2002, Vol. 20, No. 6, p. 1247–1257.

[6] S.S. Ghassemzadeh, L.J. Greenstein, A. Kavčić, T. Sveinsson & V. Tarokh "An Empirical Indoor Path Loss Model for Ultra-Wideband Channels," *KICS Journal of Communications and Networks*, 2003, Vol. 5, No. 4, p. 303–308.

[7] J. Foerster, "Channel Modelling Sub-committee; Final Report". IEEE P802.15-02/490r1-SG3a, Mar 2003.

[8] A.A.M. Saleh and R.A. Valenzuela "A Statistical Model for Indoor Multipath Propagation," *IEEE Journal on Selected Areas of Communications 5*, 1987, pp. 128–137.

[9] P. Krishnamurthy, J. Beneat, M. Marku and K. Pahlavan "Modeling of the Wideband Indoor Radio Channel for Geolocation Applications in Resi-dential Areas," *in IEEE 49th Vehicular Technology Conference*, Houston, USA, Vol. 1, 1999, pp. 175–179.